Polymer 49 (2008) 3146–3156

Contents lists available at ScienceDirect

Polymer

journal homepage: www.elsevier.com/locate/polymer

Foaming behavior of isotactic polypropylene in supercritical CO_2 influenced by phase morphology via chain grafting

Wentao Zhai [a,b], Hongying Wang [a,b], Jian Yu [a,*], Jin-Yong Dong [a,*], Jiasong He [a]

[a] Beijing National Laboratory for Molecular Sciences (BNLMS), Key Laboratory of Engineering Plastics, Joint Laboratory of Polymer Science and Materials, Institute of Chemistry, Chinese Academy of Sciences, Beijing 100190, China
[b] Graduate School, Chinese Academy of Sciences, Beijing 100039, China

ARTICLE INFO

Article history:
Received 25 March 2008
Received in revised form 14 May 2008
Accepted 15 May 2008
Available online 18 May 2008

Keywords:
Isotactic polypropylene foam
Graft
Phase morphology

ABSTRACT

Polystyrene (PS) and poly(methyl methacrylate) (PMMA) grafted isotactic polypropylene copolymers (iPP-*g*-PS and iPP-*g*-PMMA) with well-defined chain structure were synthesized by atom transfer radical polymerization using a branched iPP (iPP-B) as polymerization precursor. The branched and grafted iPP were foamed by using supercritical CO_2 as the blowing agent with a batch method. Compared to linear iPP foam, the iPP-B foams had well-defined close cell structure and increased cell density resulted from increased melt strength. Further incorporating PS and PMMA graft chains into iPP-B decreased the crystal size and increased the crystal density of grafted copolymers. In iPP-*g*-PS foaming, the enhanced heterogeneous nucleation by crystalline/amorphous interface further decreased the cell size, increased the cell density, and uniformized the cell size distribution. In contrast to this, the iPP-*g*-PMMA foams exhibited the poor cell morphology, i.e., large amount of unfoamed regions and just a few cells distributed among those unfoamed regions, although the crystal size and crystal density of iPP-*g*-PMMA were similar to those of iPP-*g*-PS. It was found that the iPP-*g*-PMMA exhibited PMMA-rich dispersed phase, which had higher CO_2 solubility and lower nucleation energy barrier than copolymer matrix did. The preferential cell nucleation within the PMMA-rich phase or at its interface with the matrix accounted for the poor cell morphology. The different effect of phase morphology on the foaming behavior of PS and PMMA grafted copolymers is discussed with the classical nucleation theory.

1. Introduction

Isotactic polypropylene (iPP) is one of the most widely used commercial polymers. It has many desirable and beneficial physical properties such as low density, high melting point, high tensile modulus, and excellent chemical resistance [1]. Those outstanding properties as well as the low material cost would make iPP being more competitive in producing polymer foam than other thermoplastics such as polyethylene and polystyrene in various industrial applications, and hence producing the well-defined iPP foams have gained growing interest in recent years [2]. However, the linear iPP exhibits poor foaming behavior due to its low viscosity and low melt strength during the foaming process, which has been shown by many researchers [3,4].

Various methods have been reported up to now to modify the chain structure with the aim to increase the melt strength and eventually improve the foamability of iPP, such as long-chain branching or grafting [5–8] and chemical or radiation crosslinking [9–11]. Among these methods, the most attractive one is the introduction of branched structure into the linear iPP, because polymers with just a few long branch chains can exhibit significant strain hardening property and high melt strength [12,13], which effectively suppress the rupture of cell walls under the elongational force acting during cell growth [6,14]. Moreover, the presence of branched structure also improves the processing properties of polymer due to the significant shear thinning property at high shear rate [15,16].

Blowing agent is another aspect to influence the foaming behavior of polymer [17]. In the recent years, supercritical CO_2 have been shown to be an attractive alternative to conventional physical blowing agents in polymer foaming [18–20], because of the environmentally benign nature and relatively mild critical conditions ($T_C = 31.1$ °C and $P_C = 7.37$ MPa) of CO_2. The existence of specific intermolecular interactions between CO_2 and polymer can increase the solubility of CO_2 in polymer [19,21,22]. For example, poly(methyl methacrylate) (PMMA) exhibits higher CO_2 solubility than iPP because of Lewis acid–base interaction between carbonyl groups and CO_2 [23,24]. According to the classical nucleation

* Corresponding authors. Tel./fax: +86 10 6261 3251.
E-mail addresses: yuj@iccas.ac.cn (J. Yu), jydong@iccas.ac.cn (J.-Y. Dong).

0032-3861/$ – see front matter © 2008 Elsevier Ltd. All rights reserved.
doi:10.1016/j.polymer.2008.05.018

theory, increasing CO_2 content in polymer tends to decrease the energy barrier and increase the rate of cell nucleation during polymer foaming process [25,26]. Therefore, it is expected that the cell morphology of iPP foam would be improved if PMMA chain were introduced into iPP.

However, there are many difficulties in preparing branched/grafted iPP samples, especially those with well-defined structure and high affinitive group [27]. In the present work, branched iPP copolymers (iPP-B) with a few pendant un-saturated groups were synthesized by copolymerizing *p*-(3-butenyl)styrene and propylene. With iPP-B as the polymerization precursor, the iPP samples with well-defined amorphous polystyrene (PS) and PMMA grafted structure were synthesized by using atom transfer radical polymerization (ATRP). The thermal and crystallization properties, and CO_2 sorption behaviors were investigated as well as a linear iPP (iPP-L). Then the polymers were foamed by using supercritical CO_2 as the physical blowing agent with a batch method. The influences of PS and PMMA graft structures on the foaming behavior of iPP samples are discussed according to the classical nucleation theory, taking into account the different phase morphology of unfoamed graft copolymers.

2. Experimental section

2.1. Materials and characterization

IPP-L sample was supplied by Lanhua Petrochemical Corporation, China. IPP-B sample was synthesized by copolymerizing *p*-(3-butenyl)styrene and propylene, as illustrated in Scheme 1. The *p*-(3-butenyl)styrene served as both comonomer and transfer agent during metallocene-mediated propylene polymerization, which used isospecific *rac*-$SiMe_2$(2-Me-4-(1-naph)Ind)$_2ZrCl_2$ catalyst in the presence of a small amount of hydrogen. In this study, three iPP-B samples with different branch densities of 1.8–3.6 branch chain/1000 carbon of backbone were synthesized and coded as iPP-B1, iPP-B2, and iPP-B3, respectively. Using iPP-B as the polymerization precursor, two series of grafted copolymers, i.e., iPP-*g*-PS and iPP-*g*-PMMA, were prepared by ATRP, as outlined in Scheme 1, and the details were shown elsewhere [28]. The grafted copolymers with different PS contents were coded as iPP-*g*-PS2 (1.9 mol%), iPP-*g*-PS7 (7.2 mol%), and iPP-*g*-PS13 (12.7 mol%), and PMMA as iPP-*g*-PMMA2 (2.5 mol%), iPP-*g*-PMMA7 (7.4 mol%), and iPP-*g*-PMMA19 (19.0 mol%). The characteristics of iPP-L, iPP-B, and grafted copolymers are shown in Table 1. It is needed to point out that the grafted copolymers synthesized from the same precursor had the same branch and graft density. For these grafted copolymers, the increase in the PS or PMMA contents indicated the increase in graft chain length. CO_2 with a purity of 99.95% was supplied by Beijing Analytical Gas Factory, China.

2.2. Sample preparation

The polymers were molded by compression at 200 °C into sheets of 1 mm and 50 μm thickness, after dried at 60 °C under vacuum for 1 week with the aim to completely remove the probable adsorbed water and solvent. The dried sample was extracted with boiling THF. And the FTIR spectrum of the extraction solution, which missed the characteristic peak of carbonyl group at 1730 cm^{-1}, confirmed that the drying process did not induce the decomposition of PMMA. The sample with thickness of 1 mm was cut into specimens with dimensions of 5×25 mm for batch foaming and that of 50 μm was used for POM observation.

2.3. Gas sorption measurement

The CO_2 sorption was measured by using commonly accepted gravimetric method. The polymer sheets were enclosed in a high-pressure vessel preheated to 50 °C. The vessel was flushed with low

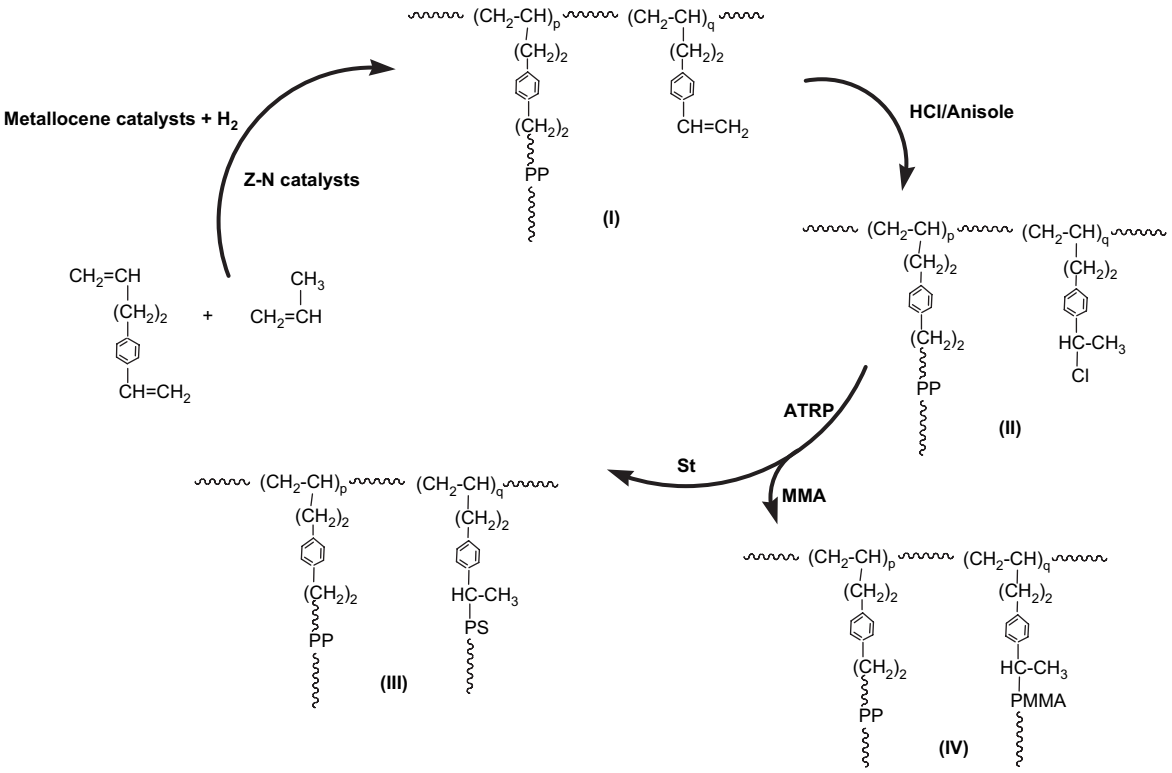

Scheme 1. The route for synthesizing iPP-B (I) and PS (III) or PMMA (IV) grafted copolymers samples.

Table 1
Physical characteristics of the linear, branched and grafted iPP samples

Sample	Graft content (mol%)	M_n (10^4 g/mol)	M_w/M_n	N_b[a]	N_g[b]	L_s[c] (10^3 g/mol)	T_m (°C)	X_c (%)
iPP-L	0	11.42	3.94	0	0	0	158.6/164.1	58.2
iPP-B1	0	3.02	1.77	1.8	0	0	151.1	48.2
iPP-*g*-PS2	1.9	3.55	2.49	1.8	0.8	1.2	150.7	44.4
iPP-*g*-PMMA2	2.5	3.57	2.34	1.8	0.8	1.6	137.9/151.0	46.7
iPP-*g*-PMMA7	7.4	3.70	2.14	1.8	0.8	5.0	137.6/150.7	40.0
iPP-B2	0	ND	ND	3.2	0	0	150.6	48.7
iPP-*g*-PS7	7.2	3.67	2.34	3.2	1.8	2.3	150.1	38.0
iPP-*g*-PMMA19	19.0	4.09	2.36	3.2	1.8	6.5	137.8/150.6	28.8
iPP-B3	0	ND	ND	3.6	0	0	147.6	47.9
iPP-*g*-PS13	12.7	3.92	2.97	3.6	2.3	3.3	146.9	24.6

ND: not determined.
[a] The average number of branch/1000 C of backbone, which was determined by means of ^{1}H NMR.
[b] The average number of graft/1000 C of backbone, which was determined by means of ^{1}H NMR.
[c] The average length of graft chain, which was calculated according to Ref. [28].

pressure CO_2 for about 3 min, then the pressure was increased to 12 MPa. The samples were saturated under this condition for 10 h to ensure equilibrium adsorption of CO_2. Then the samples were removed out following a rapid venting of the vessel, and transferred within a 1 min interval to a digital balance (sensitivity of 0.1 mg) to record mass loss as a function of time. The mass uptake of CO_2 in the high-pressure vessel was calculated by linear extrapolating the initial stage of desorption curve of CO_2. The sorption experiments were repeated three times for one condition to obtain the experimental errors of CO_2 solubility measurements.

2.4. Batch foaming

The basic process of polymer saturation with CO_2 was the same as that of gas sorption measurement. After saturation for 10 h to ensure equilibrium sorption of CO_2, the samples were removed from the vessel after a rapid quench of pressure and transferred within a 1 min interval to a silicone oil bath kept at a fixed temperature. The samples were foamed in the silicone oil bath for 20 s, then quenched in cold water.

2.5. Analysis

Molecular weight (M_n) and molecular weight distribution (M_w/M_n) of polymers were measured using a Waters Alliance GPC 2000 instrument operated at 150 °C with 1,2,4-trichlorobenzene as the mobile phase. The melting point (T_m) was determined by using a Perkin Elmer DSC-7 calibrated with indium. All operations were carried out with a heating rate of 20 °C/min over a temperature range from 50 to 200 °C under a nitrogen environment. The crystallinity was calculated from the integration of melting peak of the DSC thermogram and using the heat of fusion of 209.0 J/g for 100% crystalline PP [29]. Each sample was tested for three times. Wide-angle X-ray diffraction (WAXD) measurements were conducted on a Rigaku D/max 2500 with Cu Kα radiation (40 kV, 300 mA). The scanning angle 2θ ranged between 5° and 40° with a step scanning rate of 4° min^{-1}. Polarized optical microscope (POM) was used to show the spherulite morphology of samples. Before observation, samples were melted at 180 °C for 5 min and then isothermally crystallized at 138 °C for 30 min. The morphology of unfoamed and foamed samples was observed with a Hitachi S-530 scanning electron microscope (SEM). The samples were freeze-fractured in liquid nitrogen and sputter-coated with platinum. Energy dispersive X-ray (EDX) element analysis was carried out to study the morphology of unfoamed iPP-*g*-PMMA2. And the morphology of unfoamed iPP-*g*-PS7 sample was further characterized by transmission electron microscopy (TEM). Prior to the examination, samples were microtomed in liquid nitrogen using an ultramicrotome and chemically stained in ruthenium tetraoxide (RuO_4) vapor for 4 h. Images were obtained from a Philips CM12 apparatus using an accelerating voltage of 80 kV. The cell size and cell density of foamed samples were determined from SEM micrographs. The cell diameter was the average of sizes of at least 100 cells in the SEM micrographs. The cell density (N_0), the number of cells per cubic centimeter of solid polymer, was determined from Eq. (1) [30]:

$$N_0 = \left[\frac{nM^2}{A}\right]^{3/2}\left[\frac{1}{1-V_f}\right] \quad (1)$$

where n is the number of cells in the SEM micrograph, M the magnification factor, A the area of the micrograph (cm^2), and V_f the void fraction of the foamed sample, which can be estimated as

$$V_f = 1 - \frac{\rho_f}{\rho} \quad (2)$$

where ρ and ρ_f were the mass densities of samples before and after foaming treatment, respectively, which were measured by water displacement method according to ISO 1183-1987.

3. Results and discussion

3.1. Thermal and crystallization properties of iPP samples with different chain structures

In the batch foaming, the melting point, crystallinity, and crystal structure [1,31] of semi-crystalline polymer would affect the cell morphology of resultant foam. Therefore, the thermal and crystallization properties of iPP samples are discussed in this section.

Fig. 1 shows the DSC thermograms of iPP samples with different chain structures. In Fig. 1a, iPP-L shows two melting points, i.e., 158.6 and 164.1 °C, during the DSC heating scan. It is a well-known phenomenon which results from two major kinds of lamella with different thicknesses [32,33]. iPP-B1 with branch density of 1.8 branch chain/1000 carbon of backbone shows only a melting point at 151.1 °C. This temperature was much less than those of iPP-L, mostly because of the low molecular weight and the presence of branched structure. With increasing the branch density to 3.2 (iPP-B2) and 3.6 (iPP-B3) branch chain/1000 carbon of backbone, the melting point of iPP-B samples decreases to 150.6 and 147.6 °C, respectively, indicating a slight effect of the branch density on the

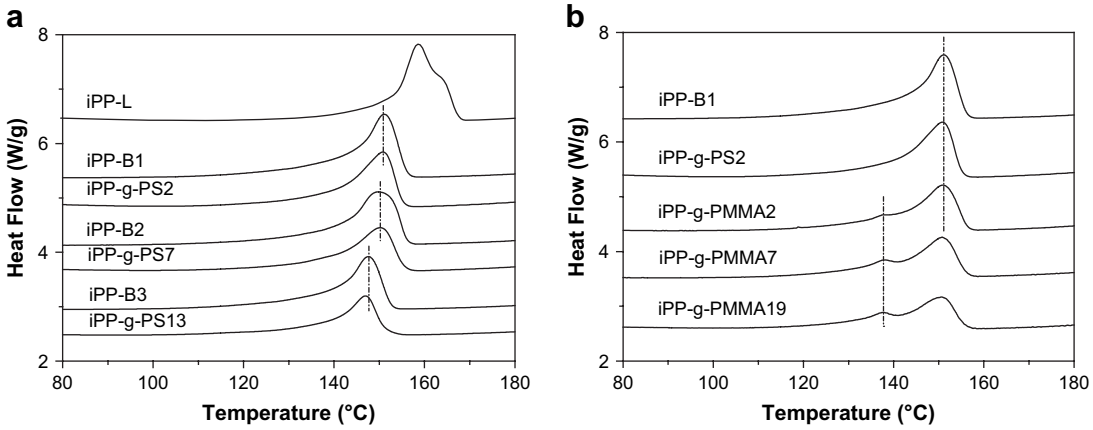

Fig. 1. DSC thermograms of the iPP-L, iPP-B, and iPP-*g*-PS samples (a), and iPP-*g*-PMMA samples (b).

melting point of iPP-Bs. With further grafting PS to iPP-Bs, the melting point of grafted copolymers changes to 150.7 °C for iPP-*g*-PS2, 150.1 °C for iPP-*g*-PS7, and 146.9 °C for iPP-*g*-PS13. Therefore, iPP-*g*-PS had similar melting point with their corresponding precursors, possibly because the PS chains were excluded to the fold surface of the lamellar structure and hence did not affect the perfection of crystallites of polymer due to the low graft density of 0.8–2.3 graft chain/1000 carbon of backbone as shown in Table 1. Similar behavior has been observed in the previous studies [34,35]. Influence of graft chain length on the melting point of iPP is shown in Fig. 1b. It is seen that the melting point of grafted copolymers is 151.0 °C for iPP-*g*-PMMA2, and 150.7 °C for iPP-*g*-PMMA7, which was similar to that of the corresponding polymerization precursor iPP-B1. Therefore, the graft polymerization and graft chain length did not significantly affect the melting point of grafted copolymers in this study.

It is noted that all the DSC thermograms of iPP-*g*-PMMA samples had a weak melting peak at about 137.8 °C (Fig. 1b), which was different from those of iPP-*g*-PS samples. WAXD measurements were conducted to illuminate the possible reason, and the results are shown in Fig. 2. The iPP-B2 and iPP-*g*-PS7 samples exhibit only the typical characteristics of α form ($2\theta = 13.9$, 16.8, 18.5, 21.2, and 21.7°), indicating that the incorporation of PS units did not change the crystal form displayed in iPP-B2. On the contrary, iPP-*g*-PMMA7 and iPP-*g*-PMMA19 have a new peak at $2\theta = 16.0°$, indicating the formation of β crystal form in both the graft copolymers although they were synthesized from different precursors. The β crystal form could be the origin of the weak peak in the DSC thermograms of iPP-*g*-PMMA samples.

Fig. 3 summarizes the results of corrected crystallinity according to the graft content (weight fraction) of iPP samples. All the branched samples have similar crystallinity, i.e., 48.2%, which is smaller than 58.2% of iPP-L. With the introduction of graft units, the corrected crystallinity changes to 46.5% for iPP-*g*-PS2, 45.2% for iPP-*g*-PS7, and 45.0% for iPP-*g*-PS13; while 47.9% for iPP-*g*-PMMA2, 47.5% for iPP-*g*-PMMA7, and 46.9% for iPP-*g*-PMMA19. These results indicate that no significant change in crystallinity was observed with different amounts of grafting amorphous PS or PMMA structure, which was in accordance with the results of melting point. It seems that the simple dilution effect governed the crystallinity of the grafted copolymers with low graft density [33].

The crystal morphology, e.g. crystal density and crystal size, of the iPP-L, iPP-B1 and grafted iPP samples was investigated by POM after isothermally crystallized at 138 °C for 30 min, and the results are shown in Fig. 4. It is found that iPP-L has the biggest crystal size, next in crystal size is iPP-B1, which is followed by grafted

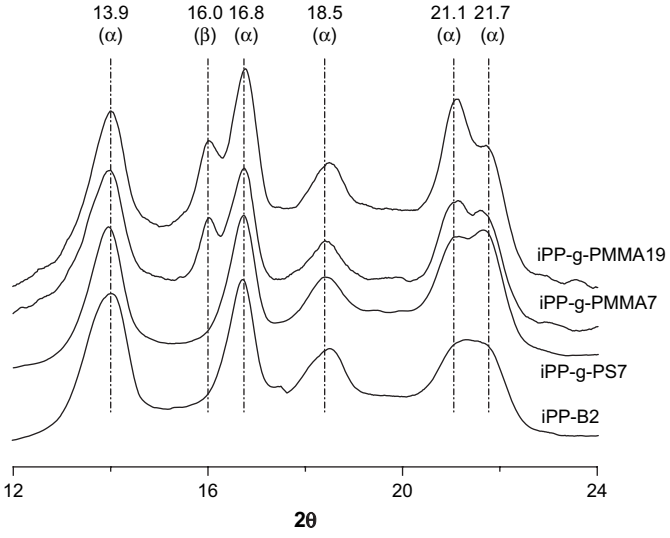

Fig. 2. WAXD curves of iPP-B2, iPP-*g*-PS7, iPP-*g*-PMMA7, and iPP-*g*-PMMA19.

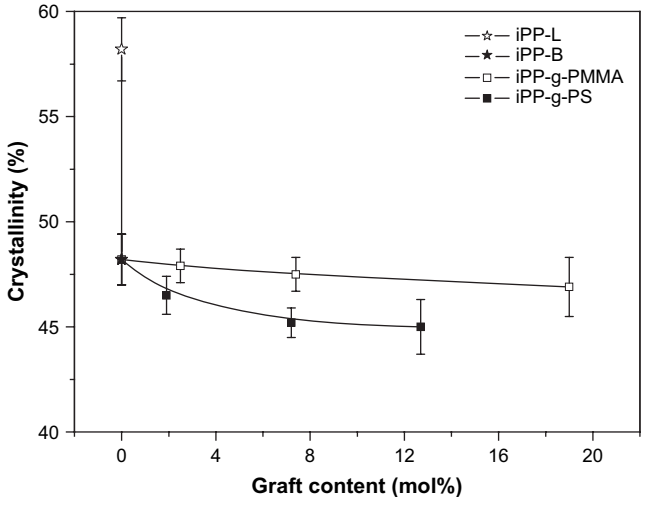

Fig. 3. Corrected crystallinity with graft content (weight fraction) of the linear, branched and grafted iPP samples.

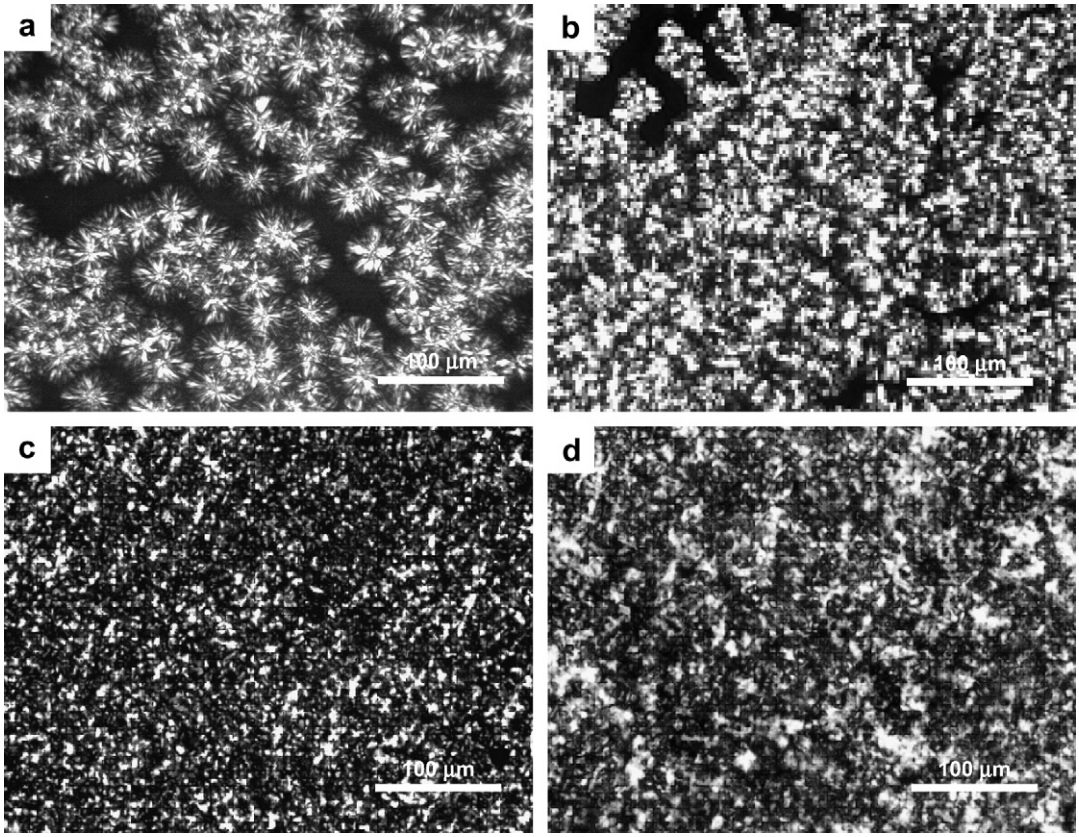

Fig. 4. POM micrographs of iPP-L (a), iPP-B1 (b), iPP-*g*-PS7 (c), and iPP-*g*-PMMA7 (d).

copolymers. Meanwhile, the crystal density has the reversed order. These results indicate that the side chains, including the branched iPP chains and grafted PS or PMMA chains, could act as the heterogeneous nucleation sites to promote the crystal nucleation, resulting in the decrease in crystal size and increase in crystal density [36,37]. Moreover, the heterogeneous nucleation effect tended to enhance with increasing the number of the side chains.

In summary, the introduction of amorphous PS or PMMA graft units did not obviously affect the melting point and crystallinity of the crystalline iPP backbone. However, the graft structure acted as the heterogeneous nucleation site to modify the crystal morphology of polymer.

3.2. Sorption of CO_2 in iPP samples

The influence of chain structure on the sorption kinetics of CO_2 was examined in iPP samples saturated at 12 MPa and 50 °C. Fig. 5a shows the percentage mass uptake of CO_2 versus the square root of desorption time for iPP-L, iPP-B1, iPP-*g*-PS7, and iPP-*g*-PMMA7 samples. A good linear relationship indicated that the diffusion of CO_2 obeys the Fick's law in these copolymers, which was identical to the desorption kinetics of other pure polymers [20]. The solubility of CO_2 in the samples was obtained by linear extrapolating desorption curve to zero desorption time. It is well known that the sorption of gas in the semi-crystalline polymer almost exclusively occurs in the amorphous regions [38,39]. Consequently, the equilibrium solubility of CO_2 in different iPP samples was calculated with the crystallinity correction, and the results are shown in Fig. 5b. The corrected solubility in iPP-B1 shows a slight increase in CO_2 sorption of 11.1% relative to 10.5% of iPP-L. With the introduction of PS units into iPP-B, the CO_2 solubility is 11.0% for iPP-*g*-PS2, 11.2% for iPP-*g*-PS7, and 11.3% for iPP-*g*-PS13. The similar solubility of CO_2 in iPP-B and iPP-*g*-PS suggests that PS units exhibited the similar CO_2 solubility with the amorphous regions of iPP-B. On the other hand, the CO_2 solubility changes to 12.7% for iPP-*g*-PMMA2, 13.6% for iPP-*g*-PMMA7, and 13.9% for iPP-*g*-PMMA19, indicating that the amorphous regions in iPP-*g*-PMMA exhibited remarkably increased CO_2 solubility relative to those in iPP-*g*-PS and iPP-B samples, which was attributed to the strong interaction between CO_2 and the electron donating carbonyl groups in PMMA [26].

3.3. Cell morphology improvement in iPP-B and iPP-g-PS foams

iPP-L, iPP-B, and iPP-*g*-PS samples were saturated at 12 MPa and 50 °C, then foamed at 170, 150, and 150 °C for 20 s, respectively. The higher foaming temperature chosen for iPP-L sample was due to its higher melting point. As shown in Fig. 6(a), iPP-L foam has the typical cell morphology of low melt strength iPP, such as open cell structure, a large amount of unfoamed regions, and very non-uniform cell size distribution. Fig. 6(b–d) shows that iPP-B with different branched degrees exhibits similar closed cell structure with broad cell size distribution after foaming. Fig. 6(e–g) shows the cell morphology of iPP-*g*-PS foams. Compared to the corresponding iPP-B foams, iPP-*g*-PS foams exhibit narrow cell size distribution with closed cell structure.

Fig. 7 shows the corresponding cell parameters of iPP-B1 and iPP-*g*-PS foams, which indicate that the introduction of PS graft chains decreases the average cell size from 17.5 μm for iPP-B1 foam to 9.5 μm for iPP-*g*-PS2 foam, 7.9 μm for iPP-*g*-PS7 foam, and 6.5 μm for iPP-*g*-PS13 foam. On the other hand, the cell density increases from 0.24×10^9 cells/cm^3 for iPP-B1 foam to 1.35×10^9 cells/cm^3 for iPP-*g*-PS2 foam, 1.95×10^9 cells/cm^3 for iPP-*g*-PS7 foam, and 2.46×10^9 cells/cm^3 for iPP-*g*-PS13 foam. Another important

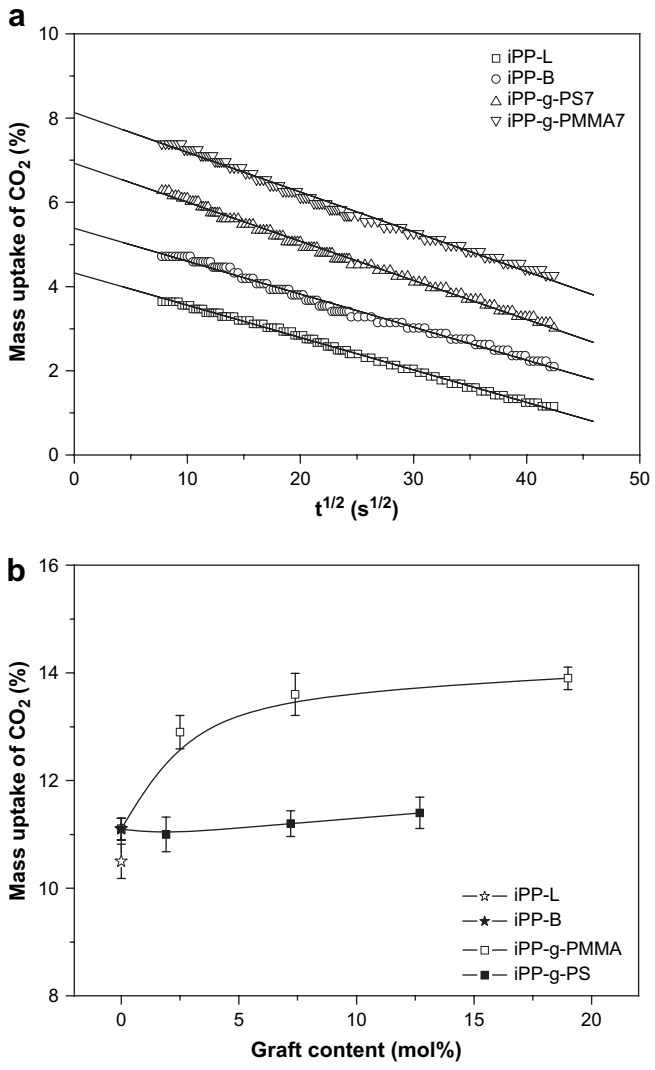

Fig. 5. Desorption curves of iPP-L, iPP-B1, iPP-*g*-PS7, and iPP-*g*-PMMA7 samples (a) and the corrected CO_2 solubility with crystallinity of the linear, branched and grafted iPP samples (b). Saturation conditions: 12 MPa and 50 °C.

feature of the iPP-*g*-PS foams is the uniform cell size distribution. As shown in Fig. 7, iPP-B1 foam shows a broad cell size distribution with cell size between 5 and 35 μm, which narrows down to 3–18 μm for iPP-*g*-PS2 foam, 3–13 μm for iPP-*g*-PS7 foam, and 2–12 μm for iPP-*g*-PS13 foam. Furthermore, the cell size tends to follow Gaussian distribution with increasing PS content. Therefore, the incorporation of PS units significantly decreased the cell size, increased the cell density, and uniformized the cell size distribution of iPP foams, and the effects became more obvious at higher PS graft content.

It is known that the melt strength of linear iPP is too weak to bear the extensional force, resulting in the serious cell coalescence and the formation of open cell structure after foaming [3,4]. The presence of branched structure in iPP-B sample obviously increased the melt strength, hence improved the foaming behavior, even though it had much lower molecular weight than that of iPP-L. With increasing the branch density from 1.8 to 3.6 branch/1000 carbon of backbone, however, no obvious improvement in cell morphology of iPP-B foams was observed, which indicates that the presence of a few long-branching structure was enough to endow iPP with high melt strength [40]. It should be pointed out that there was only 0.6% increase in CO_2 solubility for iPP-B vs. iPP-L. Compared to the increase in melt strength, this slight increase in CO_2 solubility should be less important for improving the foaming behavior of iPP-B sample.

For grafted copolymers, using iPP-B as precursor ensured their high melt strength. However, the increased melt strength could not account for the uniform cell size distribution of iPP-*g*-PS foams shown in Fig. 6(e–g). As indicated in our previous study, the foams produced from the crosslinked iPP samples with high melt strength also exhibited broad cell size distribution [41], which was attributed to the non-uniform cell nucleation during the foaming process due to the presence of large crystal regions [30,42]. It is well-established that in the case of semi-crystalline polymer foamed by a temperature rising process, the influence of crystal regions on the cell morphology mainly includes two aspects. One of them is that the crystal regions may serve as heterogeneous nucleation sites to enhance cell nucleation due to the decreased nucleation energy barrier at the phase interface [30,43,44]. The other is that the presence of crystal regions leads to the non-uniform cell nucleation because the gas does not dissolve in crystallites [31,42]. Therefore, the change of crystal size and crystal density in iPP was expected to affect the cell morphology of polymer foam. In the case of iPP-B, the large crystal size made the cell nucleation non-uniform, resulting in the broad cell size distribution in iPP-B foams. Similar phenomenon has been broadly observed in high crystallinity polymer foam [38,41,42]. In the case of iPP-*g*-PS, however, the crystals with significantly decreased size and increased density supplied much more and much uniform dispersed heterogeneous cell nucleation sites, which facilitated to obtain the foam with increased cell density and uniformized cell size distribution. This result was well consistent with our previous study [45], where the uniform dispersed nanosilica significantly narrowed the cell size distribution of polycarbonate foam. Therefore, the enhanced heterogeneous cell nucleation, resulted from the crystals with small size and high density, was the main reason for the improvement in cell morphology of iPP-*g*-PS foams.

The incorporation of PMMA units into iPP-B was expected to further improve the foaming behavior of iPP sample, because iPP-*g*-PMMA exhibited the increased CO_2 solubility in amorphous regions as well as the similar crystal size and crystal density relative to iPP-*g*-PS at the same graft level. As shown in Fig. 8, however, the cell morphology of iPP-*g*-PMMA foams exhibits a remarkable difference from that of iPP-*g*-PS foams under the same foaming condition. For iPP-*g*-PMMA2 foam, the fractural surface shows a large amount of unfoamed regions and just a few cells with size about 1–3 μm. With further increasing the PMMA content up to 19 mol%, the area of unfoamed regions decreases, and the number of cells increases significantly, but the distribution of cells is still non-uniform in polymer matrix. Therefore, these abnormal phenomena indicate that there were some reasons, besides the melt strength, crystallinity, and CO_2 solubility, for exhibiting much significant influence on the foaming behavior of iPP-*g*-PMMA samples, which will be discussed in the following section.

3.4. Influence of phase morphology on the foaming behavior of grafted copolymers

It is known that the heterogeneous nucleation is the main cell nucleation mode for the semi-crystalline polymer foaming due to the low energy barrier at crystalline/amorphous interface. The introduction of PS or PMMA units into iPP-B significantly decreased the crystal size and increased the crystal density of graft copolymer samples. If these well-dispersed crystal regions could effectively induce cell nucleation, the improved cell morphology would be observed in both kinds of grafted iPP foams. This was the case for iPP-*g*-PS foams. However, the poor cell morphology, i.e., non-uniform cell size distribution and a large amount of unfoamed regions,

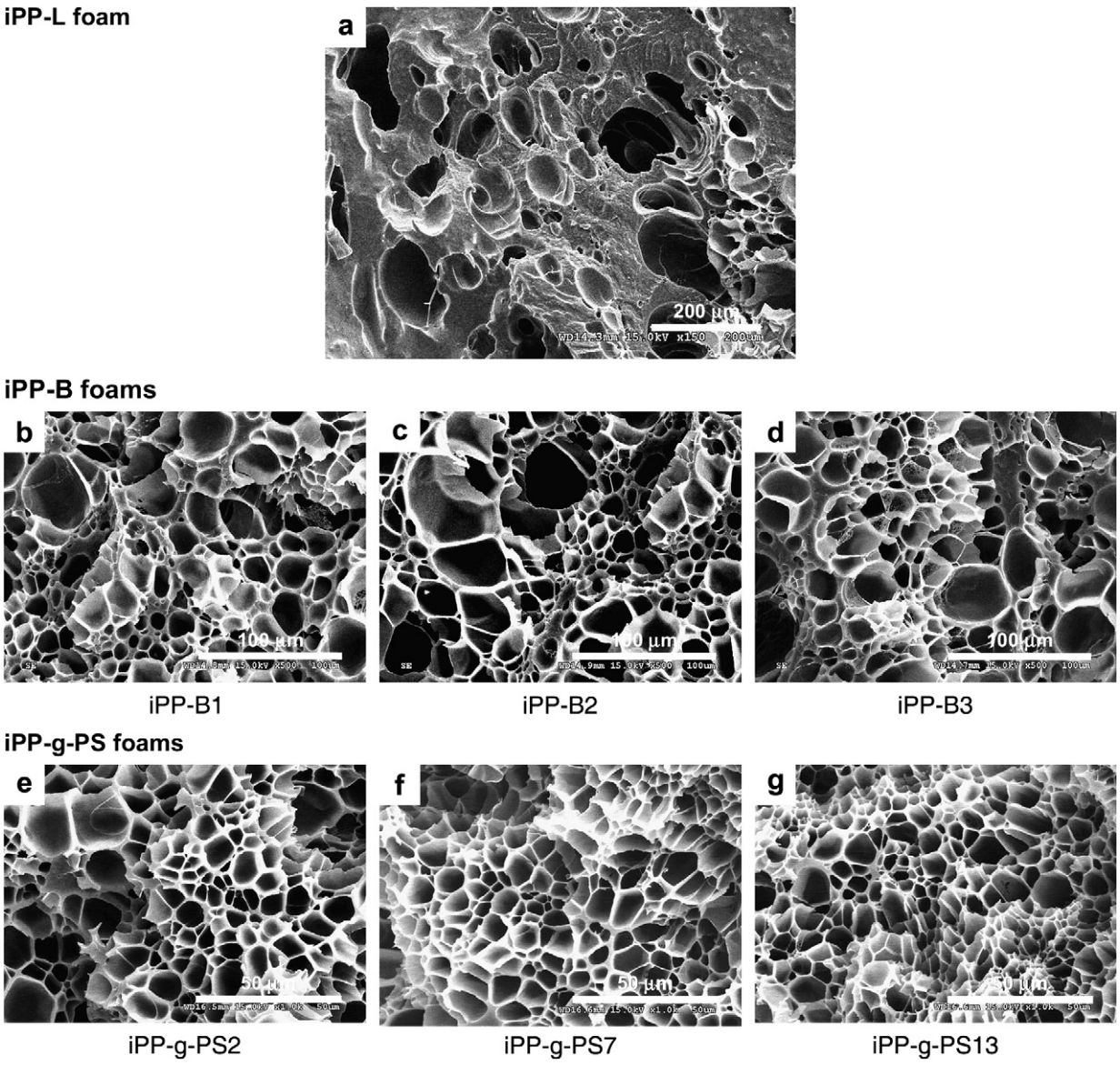

Fig. 6. The cell morphology of iPP-L (a), iPP-B (b–d), and iPP-*g*-PS (e–g) foams. Saturation conditions: 12 MPa and 50 °C; foaming conditions: 170 °C (a), 150 °C (b–d), and 150 °C (e–g) for 20 s.

was observed in iPP-*g*-PMMA foams even though the PMMA content was as high as 19 mol%. It is surprising since iPP-*g*-PMMA exhibited much higher CO_2 solubility in amorphous regions relative to iPP-*g*-PS at similar graft content. Therefore, PS and PMMA grafted copolymers displayed a different cell nucleation mechanism during the foaming process.

To investigate the origin of the different cell morphology in these foams, the grafted samples before foaming were characterized, and their SEM micrographs are shown in Fig. 9. In the case of iPP-*g*-PS shown in Fig. 9(a–c), the morphology of fractured surface is very homogeneous, and no obvious dispersed phase is observed. To further investigate the phase behavior of them, TEM was used to determine the location of PS units in RuO_4 stained iPP-*g*-PS7, and the result is shown in Fig. 10. It is known that RuO_4 preferentially stains PS over PP [46]. Similar to the SEM observation, the TEM micrographs confirmed the homogeneous distribution of PS in the polymer. On the contrary, in the case of iPP-*g*-PMMA shown in Fig. 9(d–f), the obvious globule particles with size about 140 nm are observed in iPP-*g*-PMMA2, and the size gradually increases with PMMA content, i.e., 152 nm for iPP-*g*-PMMA7 and 174 nm for iPP-*g*-PMMA19. Meanwhile, the particle density also increases with increasing PMMA graft content. These results indicate that iPP-*g*-PMMA samples exhibited obvious phase separation in the present study. EDX was used to determine the location of PMMA units in iPP-*g*-PMMA2 according to the oxygen atom content, and the result is shown in Fig. 11. Semi-quantitative analysis by EDX revealed the presence of O with content of 18.8 wt% in the particle and 4.8 wt% in the matrix, indicating that the dispersed phase was PMMA-rich.

The PMMA-rich phase might originate from the phase separation of two possible PMMA existing in the matrix, i.e., PMMA homopolymer and grafted PMMA chain. The former might come from the polymerization because of homopolymerization and/or the drying process because of degradation. The iPP-*g*-PMMA7 film (50 μm thickness) after drying process was extracted by boiling THF to investigate the probable existence of PMMA homopolymer. There was no characteristic signal of carbonyl group at 1730 cm^{-1} for the extraction solution after 15 h extraction (result not shown here). Moreover, the top surface morphology of extracted iPP-*g*-PMMA7 sample was investigated by using SEM along with non-extracted one. As shown in Fig. 12a, the surface of the extracted

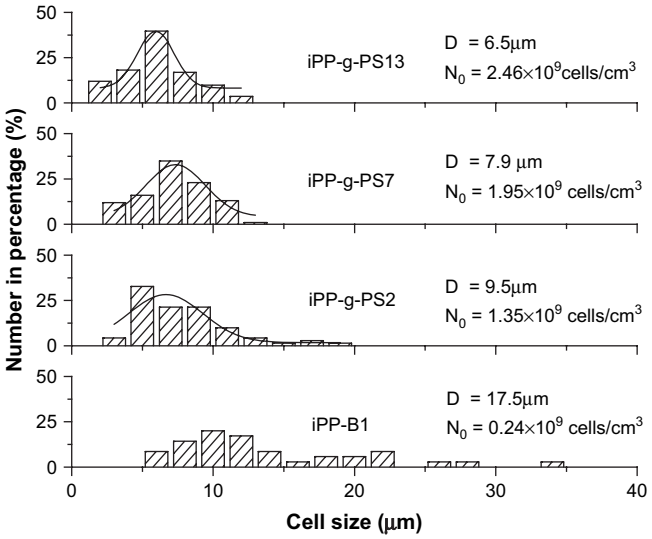

Fig. 7. Cell parameters and cell size distribution of iPP-B1 and iPP-*g*-PS foams. Saturation conditions: 12 MPa and 50 °C; foaming conditions: 150 °C for 20 s.

sample did not show obvious holes, which was similar to the top surface (Fig. 12b) and the fractured surface (shown in Fig. 9e) of the non-extracted one. These results verified no extractable PMMA homopolymer in the copolymer. Therefore, it was PMMA grafting that brought about the different phase morphology from PS grafting. The fact that iPP/PS pair has better miscibility than iPP/PMMA has been broadly verified by the much low interfacial tension of iPP/PS relative to that of iPP/PMMA [47–49].

According to the classical nucleation theory [50–52], the nucleation rate of cells per unit volume (N_0) during polymer foaming can be written as:

$$N_0 = Cf \exp\left(-\Delta G^*/k_B T\right) \tag{3}$$

where C is the concentration of CO_2 in polymer, f is the collision frequency of CO_2 molecules, k_B is the Boltzmann constant and T denotes absolute temperature. The energy barrier for cell nucleation (ΔG^*) is related to the interface tension of polymer/CO_2 (γ_{mix}) by

$$\Delta G^* = \frac{16\pi\gamma^3}{3\Delta P^2} f(\theta) \tag{4}$$

where ΔP represents the magnitude of the pressure quench during depressurization and $f(\theta)$ represents the corrected factor of heterogeneous nucleation.

It is very difficult to measure γ_{mix} at high temperature and high pressure. In the present study, the γ_{mix} was calculated according to the method reported by Goel and Beckman [53], where the surface tension of pure supercritical CO_2 was defined to be zero.

$$\gamma_{mix} = \gamma_{polymer}\left(\frac{\rho_{mix}}{\rho_{polymer}}\right)^4 (1 - w_{gas})^4 \tag{5}$$

$$\gamma_{polymer} = \gamma_c (1 - T/T_c)^{11/9} \tag{6}$$

where $\gamma_{polymer}$ is the surface tension of polymer, $\rho_{polymer}$ and ρ_{mix} are the mass densities of polymer and polymer/CO_2 mixture, respectively, w_{gas} is the weight fraction of CO_2 absorbed in the polymer, and γ_c is the surface tension of polymer at the critical temperature (T_c). Values for γ_c and T_c of the polymers are obtained from Ref. [54].

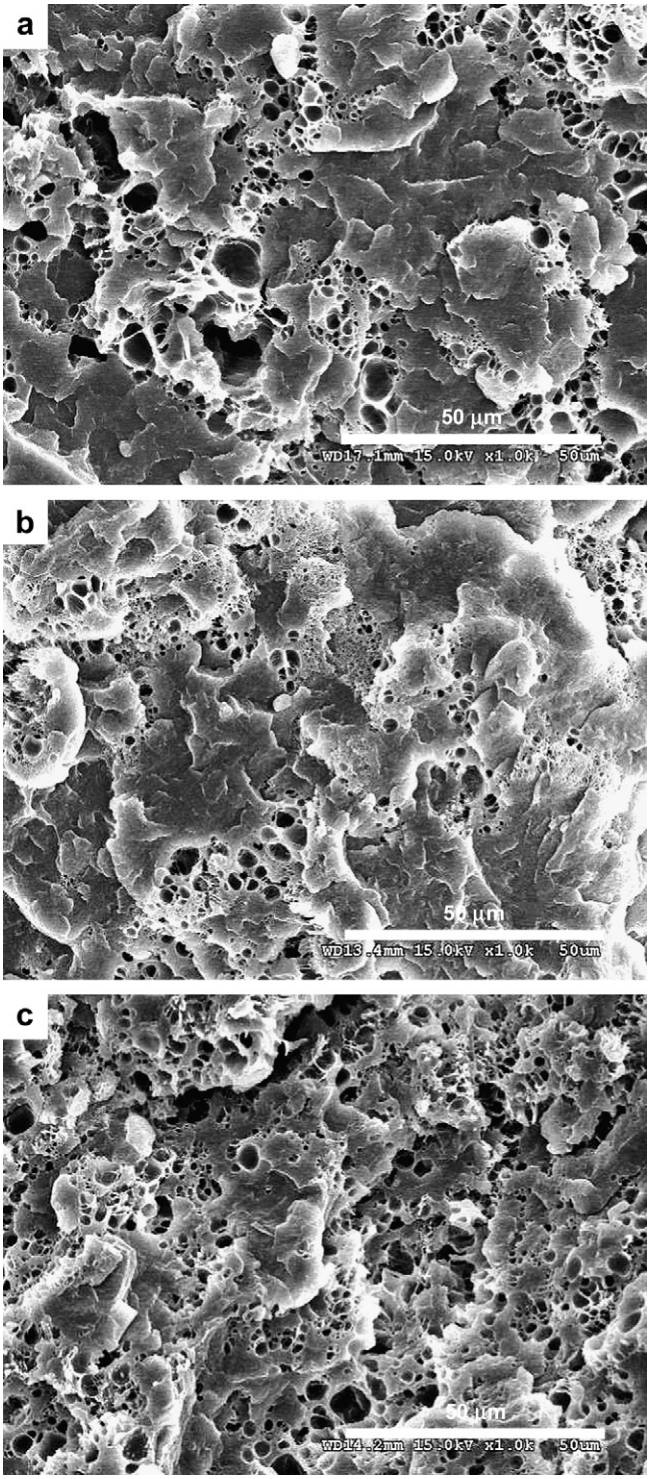

Fig. 8. SEM micrographs of iPP-*g*-PMMA2 (a), iPP-*g*-PMMA7 (b), and iPP-*g*-PMMA19 (c) foams. Saturation conditions: 12 MPa and 50 °C; foaming conditions: 150 °C for 20 s.

The foaming conditions and corresponding literature values of various parameters are listed in Table 2. Therefore, γ_{mix} was calculated from Eqs. (5) and (6) to be 15.9 mN/m for iPP/CO_2, 14.2 mN/m for PS/CO_2, and 8.8 mN/m for PMMA/CO_2. The interfacial tensions reported in other literatures are also shown in Table 2. As shown in Table 2, iPP/CO_2 and PS/CO_2 exhibit the similar interfacial tension. According to Eq. (4), PS had similar energy barrier for cell nucleation with the amorphous regions of iPP, which was higher

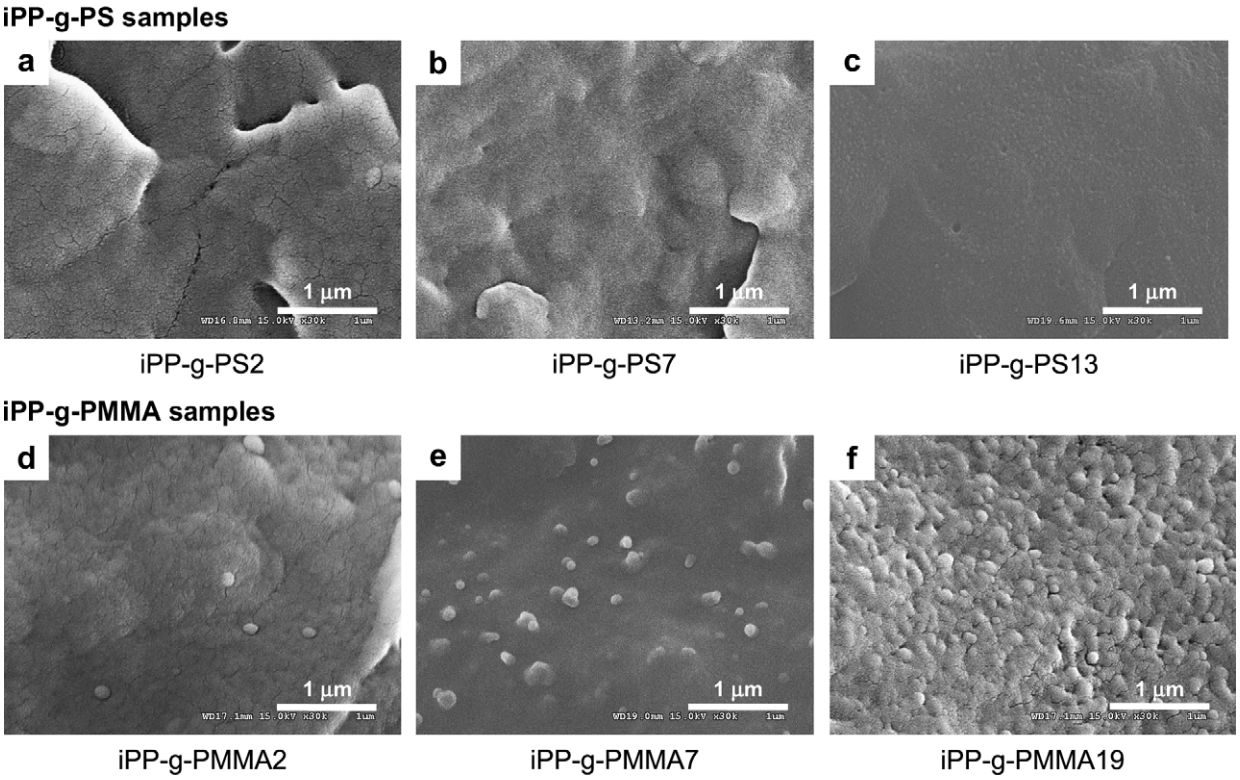

Fig. 9. SEM micrographs of the fractured surfaces of the iPP-*g*-PS (a–c) and iPP-*g*-PMMA (d–f) samples.

than that of the heterogeneous nucleation occurring at crystalline/amorphous interface during the iPP-*g*-PS foaming process. Accompanied by large numbers of small crystals, the heterogeneous nucleation facilitated the uniform distribution of cell size in iPP-*g*-PS foams. On the contrary, PMMA graft chains tended to form a dispersed phase, which had low energy barrier for cell nucleation than iPP phase because PMMA/CO_2 exhibited much lower interfacial tension than that of iPP/CO_2. Therefore, the cell nucleation preferred to occur inside the PMMA-rich phase or at the interface with iPP. Similar cell nucleation behavior has been verified [60–62] during the foaming of polymer systems with CO_2-philic polymer domains. With the occurring of cell nucleation in dispersed phase, the absorbed CO_2 in iPP phase tended to diffuse into the formed cells because of its thermodynamically favored nature [51]. According to Eqs. (4) and (5), the increased interfacial tension of iPP/CO_2 resulted from the decrease in CO_2 content [58] would further increase the energy barrier for cell nucleation. Consequently, the potential cell nucleation in iPP phase was inhibited to

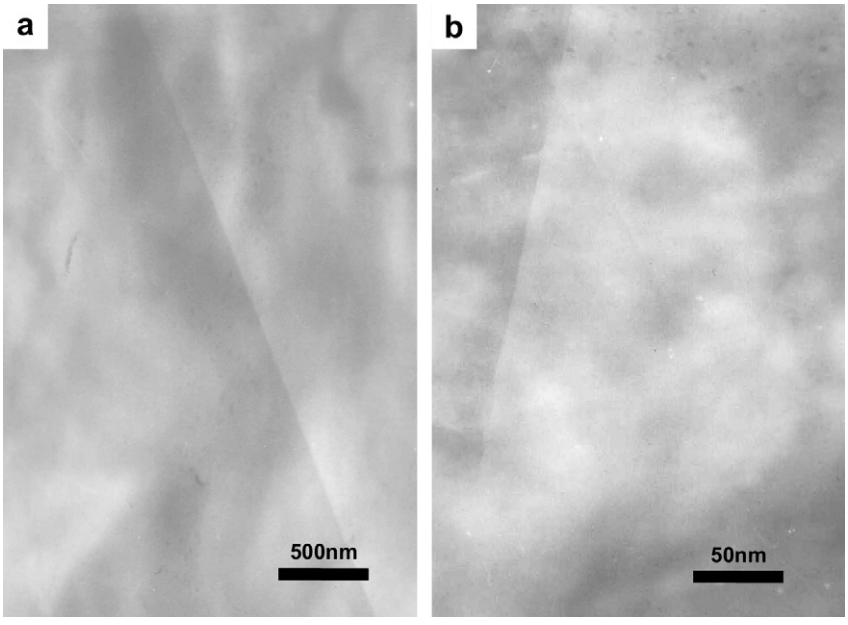

Fig. 10. TEM micrographs of iPP-*g*-PS7 sample with different magnifications.

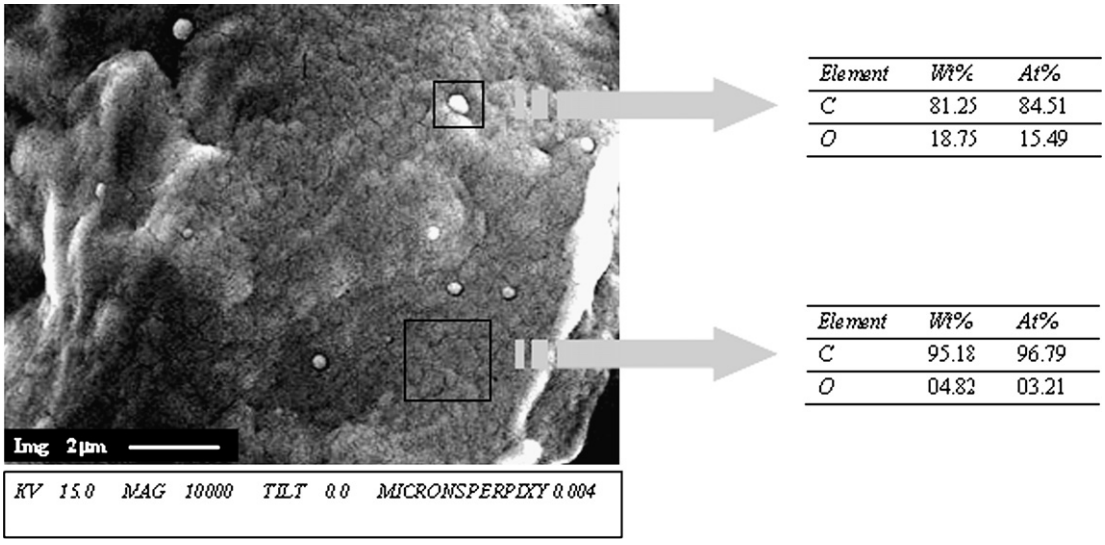

Fig. 11. SEM micrograph of fractured surfaces of the iPP-*g*-PMMA2 sample and the corresponding EDX results.

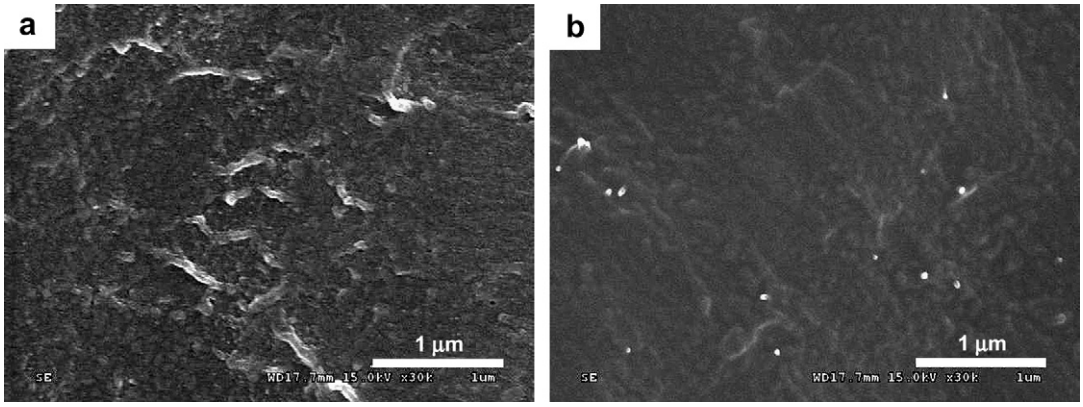

Fig. 12. SEM micrographs of the surface of iPP-*g*-PMMA7 copolymer film with (a) and without THF extraction (b).

Table 2
Calculating interfacial tension of polymers at the foaming condition[a]

Polymer	γ_c[b] (mN/m)	T_c[b] (K)	$\gamma_{polymer}$[c] (mN/m)	$\rho_{polymer}$[d] (g/cm^3)	ρ_{mix}[e] (g/cm^3)	w_{gas} (wt%)	γ_{mix} (mN/m)	
							Calculated[i]	Literature
PP	47.2	914	22.1	0.9	0.86[f]	4.3	15.9	14.1[j]
PS	63.3	967	30.7	1.0	0.90[g]	7.8[h]	14.2	13.5[k]
PMMA	65.1	935	31.2	1.0	0.82[g]	11.0[h]	8.8	–

[a] Saturation conditions: 50 °C and 12 MPa; foaming temperature: 150 °C.
[b] Obtained from Ref. [54].
[c] Calculated according to Eq. (6), where $T = 150$ °C.
[d] Estimated according to the corresponding values at ambient pressure and room temperature.
[e] Calculated from the volume expansion of polymer sample in supercritical CO_2.
[f] Obtained from Ref. [55].
[g] Obtained from Ref. [56].
[h] Obtained from Ref. [57].
[i] Calculated according to Eqs. (5) and (6).
[j] Obtained from Ref. [58], where $P = 10.5$ MPa and $T = 180$ °C.
[k] Obtained from Ref. [59], where $P = 10.5$ MPa and $T = 210$ °C.

form unfoamed regions, which was well consistent with the experimental results shown in Fig. 8. Therefore, the PMMA-rich phase in iPP-*g*-PMMA obviously changed the cell nucleation mechanism in foaming process, which accounted for the poor cell morphology.

4. Conclusions

In the present paper, the foaming behavior of linear, branched, and grafted iPP samples were investigated by using a temperature rising process with supercritical CO_2 as physical blowing agent. The grafted iPP copolymers with well-defined graft density and graft content provided a possibility to investigate the effect of chain structure on the foaming behavior of iPP. The iPP-B foam exhibited well-defined close cell structure and increased cell density relative to the linear one, attributing to the increased melt strength. The heterogeneous nucleation for crystallization by the graft chains decreased the crystal size and increased crystal density. The iPP-*g*-PS copolymer did not exhibit PS-rich dispersed phase, and the heterogeneous cell nucleation occurring at the crystalline/amorphous interface improved the cell morphology of iPP-*g*-PS foams, i.e., the gradually decreased cell size, increased cell density, and uniformized cell size distribution with further increasing the PS graft content. On the contrary, the existence of PMMA-rich dispersed phase in the iPP-*g*-PMMA copolymers resulted in the poor cell morphology, although it increased the CO_2 solubility. The cell nucleation within the PMMA-rich phase or at the phase interfaces with matrix was favored over that within the iPP phase because PMMA/CO_2 showed much less interfacial tension than that of iPP/CO_2. The enhanced cell nucleation and the following cell growth depleted most of CO_2 in the polymer, and hence inhibited the cell

nucleation in iPP phase, resulting in the unfoamed regions in iPP-*g*-PMMA foam. Meanwhile, the low content of grafted amorphous chains, which improves the foaming behavior of iPP, does not sacrifice the physical properties of polymer, such as melting point and crystallinity. Therefore, the grafted iPP should have great potential in many applications that use foaming technology.

Acknowledgements

The authors thank the Innovation Funds of CAS (no. CMS-CX200414), and the National Natural Science Foundation of China (no. 20734002) for financial support.

References

[1] Vasile C, Seymour RB. Handbook of polyolefins. New York: Marcel Dekker; 1993.
[2] Colton JS. Mater Manuf Proc 1989;4:253–62.
[3] Burt JG. J Cell Plast 1978;14:341–5.
[4] Park CB, Cheung LK. Polym Eng Sci 1997;37:1–10.
[5] Rodríguez-Pérez MA. Adv Polym Sci 2005;184:97–126.
[6] Spitael P, Macosko C. Polym Eng Sci 2004;44:2090–100.
[7] Bradley MB, Phillips EM. SPE ANTEC Tech Papers 1990;36:717–20.
[8] Naguib HE, Park CB, Panzer U, Reichelt N. Polym Eng Sci 2002;42:1481–92.
[9] Liu C, Wei D, Zheng A, Li Y, Xiao H. J Appl Polym Sci 2006;101:4114–23.
[10] Han DH, Jang JH, Kim HY, Kim BN, Shin BY. Polym Eng Sci 2006;46:431–7.
[11] Danaei M, Sheikh N, Taromi FA. J Cell Plast 2005;41:551–62.
[12] Gabriela C. J Rheol 2003;47:619–30.
[13] Wagner MH, Bastian H, Hachmann P, Meissner J, Kurzbeck S, Munstedt H, et al. Rheol Acta 2000;39:97–109.
[14] Pop-Lliev R, Liu F, Liu G, Park CB. Adv Polym Sci 2003;22:280–96.
[15] Liu CY, Li CX, Chen P, He JS, Fan QR. Polymer 2004;45:2803–12.
[16] Graebling D. Macromolecules 2002;35:4602–10.
[17] Suh KW, Park CP, Maurer MJ, Tusim MH, De Genova R, Broos R, et al. Adv Mater 2000;12:1779–89.
[18] Cooper AI. J Mater Chem 2000;10:207–34.
[19] Nalawade SP, Picchioni F, Janssen LPBM. Prog Polym Sci 2006;31:19–43.
[20] Tomasko DL, Li H, Liu D, Han X, Wingert MJ, Lee LJ, et al. Ind Eng Chem Res 2003;42:6431–56.
[21] Kirby CF, McHugh MA. Chem Rev 1999;99:565–602.
[22] Rindfleisch F, DiNoia TP, McHugh MA. J Phys Chem 1996;100:15581–7.
[23] Kamiya Y, Mizoguchi K, Terada K, Fujiwara Y, Wang JS. Macromolecules 1998;31:472–8.
[24] Kazarian SG, Vicent MF, Bright FV, Liotta CL, Eckert CA. J Am Chem Soc 1996;118:1729–36.
[25] Wang J, Cheng XG, Yuan MJ, He JS. Polymer 2001;42:8265–75.
[26] Arora KA, Lesser AL, McCarthy TJ. Macromolecules 1998;31:4614–20.
[27] Chung TC. Prog Polym Sci 2002;27:39–85.
[28] Cao C, Zou J, Dong JY, Hu Y, Chung TC. J Polym Sci Part A Polym Chem 2005;43:429–37.
[29] Wunderlich B. Crystal structure, morphology, defects. In: Macromolecular physics, vol. 1. NewYork: Academic Press; 1973.
[30] Kumar V, Suh NP. Polym Eng Sci 1990;30:1323–9.
[31] Doroudiani S, Park CB, Korschot MT. Polym Eng Sci 1996;36:2645–62.
[32] Mezghani K, Camphell RA, Phillips PJ. Macromolecules 1994;27:997–1002.
[33] Chung TC, Rhubright D, Jiang GJ. Macromolecules 1993;26:3467–71.
[34] Zhang L, Fan G, Guo C, Dong JY, Hu Y, Huang M. Polym J 2006;55:675–80.
[35] Li H, Zhao H, Zhang X, Lu Y, Hu Y. Eur Polym J 2007;43:109–18.
[36] Zhai WT, Yu J, Ma WM, He JS. Macromolecules 2007;40:73–80.
[37] Yu J, He JS. Polymer 2000;41:891–8.
[38] Park CB, Baldwin DF, Suh NP. Polym Eng Sci 1995;35:432–40.
[39] Sha H, Harrison IR. J Polym Sci Part B Polym Phys 1992;30:915–22.
[40] Lanston JA, Colby RH, Chung TC, Shimizu F, Suzuki T, Aoki M. Macromolecules 2007;40:2712–20.
[41] Zhai WT, Wang HY, Yu J, Dong JY, He JS. Polym Eng Sci. doi:10.1002/pen.21095.
[42] Lips PAM, Velthoen IW, Dijkstra PJ, Wessling M, Feijen J. Polymer 2005;46:9396–403.
[43] Baldwin DF, Park CB, Suh NP. Polym Eng Sci 1996;36:1446–53.
[44] Baldwin DF, Park CB, Suh NP. Polym Eng Sci 1996;36:1437–45.
[45] Zhai WT, Yu J, Wu LC, Ma WM, He JS. Polymer 2006;47:7580–9.
[46] Trent JS, Scheinbeim JI, Couchman PR. Macromolecules 1983;16:589–98.
[47] Valera TS, Morita AT, Demarquette NR. Macromolecules 2006;39:2663–75.
[48] Palmer G, Demarquette NR. Polymer 2005;46:8169–77.
[49] Calvão PS, Yee M, Demarquette NR. Polymer 2005;46:2610–20.
[50] Colton JS, Suh NP. Polym Eng Sci 1987;27:485–92.
[51] Colton JS, Suh NP. Polym Eng Sci 1987;27:493–9.
[52] Colton JS, Suh NP. Polym Eng Sci 1987;27:500–3.
[53] Goel SK, Beckman EJ. AIChE J 1995;41:357–67.
[54] Wu S. Polymer interface and adhesion. New York: Marcel Dekker; 1982.
[55] Lei Z, Ohyabu H, Sato Y, Inomata H, Smith RL. J Supercrit Fluids 2007;40:452–61.
[56] Pantoula M, Schnitzler J, Eggers R, Panayiotou C. J Supercrit Fluids 2007;39:426–34.
[57] Pantoula M, Panayiotou C. J Supercrit Fluids 2006;37:254–62.
[58] Li H. MS thesis. Chemical Engineering Department, The Ohio State University; 2004.
[59] Li H, Lee LJ, Tomasko DL. Ind Eng Chem Res 2004;43:509–14.
[60] Li L, Yokoyama H, Nemoto T, Sugiyama K. Adv Mater 2004;16:1226–9.
[61] Li L, Nemoto T, Sugiyama K, Yokoyama H. Macromolecules 2006;39:4746–55.
[62] Spitael P, Macosko CW, McClurg RB. Macromolecules 2004;37:6874–82.